PARTICLE SWARM OPTIMIZATION AND CFD ANALYSIS OF A HEAT SINK FOR FORCED CONVECTIVE COOLING OF A DC/AC INVERTER

Francis Onoroh[1]*, Larry Orobome Agberegha[2] and Adeyinka Abdulquadri Oluwo[1]

[1]Department of Mechanical Engineering, University of Lagos Akoka, Lagos, Nigeria

[2]Department of Mechanical Engineering, Federal University of Petroleum Resources, Delta state, Nigeria

*Corresponding email: fonoroh@unilag.edu.ng

Article history
Received
21st September 2023
Revised
16th November2023
Accepted
19th November 2023
Published
17th June 2024

ABSTRACT

Power inverters play a crucial role in converting DC voltage and current to AC voltage and current. Its efficient operation relies on effective thermal management of the semiconductor devices, such as the IRF 3205 MOSFET chip which facilitate the switching operations to prevent thermo-mechanical stress that could to failure. This research developed and optimize a heat sink for an IRF 3205 MOSFET chip in a 3.5 KVA power inverter, using the Particle Swarm Optimization technique and experimented with a 3.5 KVA 24 V power inverter operating a 1.5HP air-conditioning unit. The heat sink geometry has 26 fins, 4 mm fin thickness, 40 mm fin height, 3 mm fin spacing, 2 mm fin base thickness, 179 mm length, 80 mm width and a thermal resistance of 60.75 °C/W. The thermal performance was evaluated using Computational Fluid Dynamics (CFD) and results showed maximum base temperature of 65.85°C and experimental temperature of 64°C after two hours of steady operation dissipating heat of 45W. The results from both numerical and experimental data demonstrate the effectiveness of the optimized heat sink in maintaining the chip's temperature below its maximum working threshold of 170°C.

Keywords: *Heat sink, power inverter, thermo-mechanical stress, failure, dissipation*

1.0 INTRODUCTION

Devices, appliances, and various equipment have become crucial components of our civilization as the globe enters a more digital era. However, as the component size shrinks because of smaller designs and lean manufacturing, there is a dramatic increase in the heat flux per unit area. As a result, the working temperature of the electronic components may be higher than the desired temperature level because all electronic and power devices dissipate heat while they are in operation. During operation IRF 3205 MOSFET power modules vulnerable position is the connection part of the package structure. The degradation failure induce by high temperature is the main factor affecting the reliable operation of the DC/AC power inverter. As a result, there is the need to cool power modules in order to maintain high efficiency and prevent damage. By providing sufficient heat dissipation through extended surfaces which provide low thermal resistance, a heat sink prevents overheating and eventual damage of the component or the power inverter [1].

Most times, natural convection which involves air moving at a modest speed—is used to cool small electronic components and assemblies. Laminar convection is typically caused by the combination of tiny dimensions, the use of air as the cooling fluid, and low velocities, which leads to correspondingly low values for heat transfer coefficients. The process of forced convection with cooling fans, on the other hand, has been used to address this problem. Heat transmission is improved by actively increasing airflow speed.

Also, with these new developments and as components keep getting smaller, it is clear to note that even more heat would be dissipated from electronic components and cooling techniques must continually be improved [2]. The area for heat dissipation has decreased as electronic equipment has become more portable. As the thermal load on electronic equipment has increased, it is necessary to utilize a thermal management system, like a heat sink, to ensure that an electrical equipment runs within acceptable temperature limits and to maximize the system's efficiency in the available area [3, 4].

To lower temperatures in electrical equipment, heat sinks are frequently employed to transfer heat from heated surfaces into moving fluids. A DC to AC converter uses switches that generate heat that needs to be promptly dissipated to run efficiently and continuously. To minimize the overall form factor, heat sink designs must be optimized to reduce size and material costs [5]. Additive printing can be a useful method for creating heat sinks that match or out perform traditional aluminum heat sinks in terms of thermal performance because of its geometric flexibility, capacity for creating intricate inner structures, and high total surface to volume ratio [6].

With a power inverter, electrical power is transformed from levels of direct voltage and current to levels of alternating voltage and current. Power electronics is obviously a crucial component of power generation and engineering since about 25% of all generated power is passed through some form of electronic system. The dissipation of thermal energy in the form of heat is due to the inversion process of the MOSFETs of a power inverter. This generated heat, if not controlled, managed or prevented proves to be a real threat to the functionality, efficiency, reliability and durability of the device. As such, there is the need to design and improve cooling methods for power inverters. By changing the heat sink's form and material, it can be made more efficient. It is necessary to optimize the heat sink shape so that the predicted junction temperature of the switches does not exceed the required junction temperature, as geometry is one of the more adjustable alternatives.

In line and staggered arrays plate fins, strip fins, square pins and circular pins were all tested by Jonsson and Moshfegh [7] to see how they affect the Nusselt number and pressure drop. They discovered that Nusselt number and pressure drop are influenced by the height, thickness and spacing of the pins as well as the height and breadth of the wind tunnel with the plate fins exhibiting the lowest pressure drop and the square perforated heat sinks having a higher pressure.

An investigation was carried out by Arularasan and Velraj [8] with the goal of choosing the best heat sink design. They performed a computational fluid dynamics analysis that considered the heat sink geometry, while maintaining a consistent heat sink's length and width. They found that variables like thermal conduction resistance, heat source location and concentration, heat sink size, and airflow bypass conditions had an impact on the thermal efficiency of heat sinks and overall cooling performance.

In order to increase the rate of heat transfer in heat sinks using forced convection, Shadlaghani et al. [9] looked for a suitable pattern for the improved design of the fins used in heat sinks. The cross-sectional size and form of the fins were tuned to improve heat transfer and maintain a constant fin volume. The finite volume method and the CFD tool were used to discretize the Naiver-Stokes and energy equations. A fin with a triangle cross section transmitted heat more quickly than one with a rectangular or trapezoidal cross section at the same fin base area. The results showed that the rate of heat transmission increased as the height to thickness ratio rose.

Jaffal [10] used a mixture of experimental and computational studies to conduct the analysis and thermal evaluation of different fin heat sink geometries and specific heat flux range of from 3954 to 38357 W/m^2 with Reynolds number of 23597 to 3848.9. This study revealed that with an increasing value of free stream velocity there was a similar increase in heat transfer coefficient and a resultant decrease in thermal resistance. The study also discovered that Reynolds number significantly impacts the system's overall thermal performance and that heat transfer coefficient and thermal resistance both depend on heat flow.

In a comparable investigation, Ibrahim et al. [11] employed computational fluid dynamics (CFD) to examine the impact of heat sink geometry, rectangular, specifically circular, and triangular shapes, on the heat transfer characteristics of perforated fin heat sinks operating under various boundary conditions. They found out that forced convection heat transfer performance is significantly impacted by the perforations.

In order to achieve low thermal resistance and minimal pressure drop, Kulkarni and Dotihal [12] performed CFD and conjugate heat transfer study for various fin geometries using zigzag, fluted, slanted mirror, customized pin fin, and staggered array configurations. Base plate thickness of 2 mm, fin height of 28 mm, and fin thickness of 1 mm for three distinct heat loads, namely 50 W, 75 W, and 100 W, with a flow rate of 3.933 m/s, and air inlet temperature of 25°C, were some of the consistent and common factors in their investigation. The study found that a fin with slanted mirror geometry provides the greatest efficiency amongst all of the other geometries for minimal heat sink thermal performance when comparing the findings for the other geometries.

The majority of electronic devices use cooling techniques, which typically involve a heat sink in active or passive cooling method, according to Mjallal et al.'s [13] investigation into how heat affects electronic devices, how it increases the failure rates of the devices, and how it increases the temperature of the devices. The dimensions 20x20x6 mm were used for the experimental simulation and modeling of the heat sink. The chip and heat sink were both designed using Solid Works, while ANSYS Fluent was used for the numerical simulation. It was discovered that active cooling greatly lowers the heat sink's temperature by simulating the variation in temperature of the heat sink walls as a function of time under both passive and active cooling methods and analyzing the findings. From the reviewed literature, some work has been done on heat sink optimization with the sole aim of efficient heat dissipation but not much has been reported on optimizing heat sink geometry using the Particle Swarm Optimization (PSO) technique. Most of the reports focused on computational fluid dynamics approach to thermal performance of the heat sink. This research aim to optimize a heat sink geometry for rapid dissipation of heat in DC to AC switches utilized in power inverter analytically, numerically and experimentally test it thermal performance.

2.0 THERMALLY INDUCED POWER MODULE FAILURE MODES

Power inverter fails when the switches utilize in its construction are exposed to excessive temperatures beyond the allowable maximum junction temperature. High temperature induce thermo-mechanical stress as a result of differences in coefficient of thermal expansion of the bond materials, solder and silicon devices, common thermally induce failure modes are:

2.1 Bond Wire Failure

This failure mode is as shown in figure 1. This is largely due to the different coefficient of thermal expansion between the aluminium bond wire and the silicon device inducing mechanical stress in the bond zone [14].

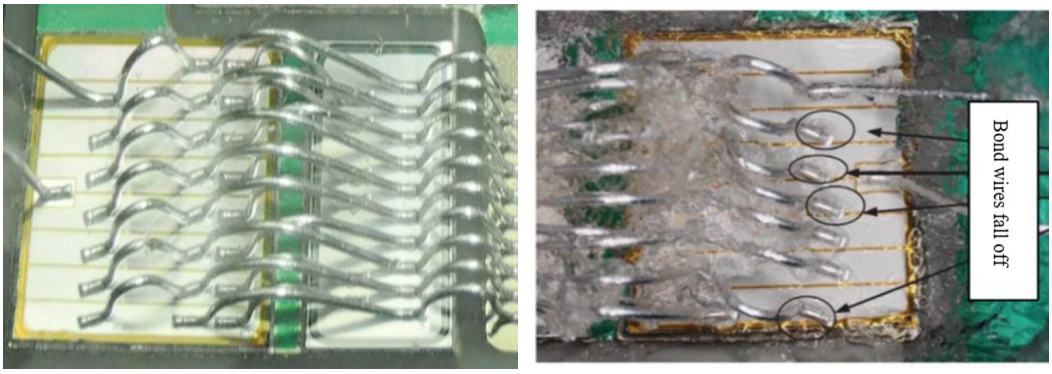

Figure 1: (left) Aluminium bonding wires (right) Bond Wire fall off [14]

2.2 Degradation of Solder Layer

Figure 2 illustrate this failure mode of switches due to temperature cycling. Mechanical stress lead to growth of voids that inhibit heat flow from the device to the heat sink resulting in excessive temperature [15].

2.3 Aging of Direct Bonded Copper Substrates (DBC)

Figure 3 shows this failure mode in detail. The industry standard for circuit boards for power modules is direct bonded copper (DBC). As shown in figure 4, thermally induced stress can result in the delamination of the metal from the substrate due to fractures and voids caused by CTE mismatches between copper and ceramic. Circular thermal stressing of DBC substrates reduces the metallization's adherence to the ceramic, which eventually results in the copper foils peeling off or delamination of copper metallization [16].

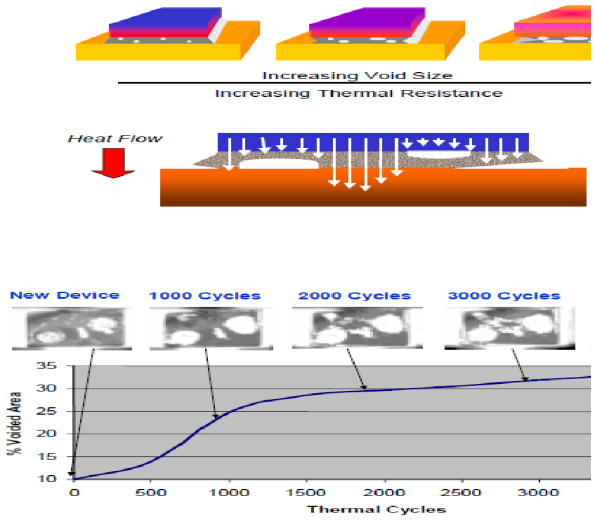

Figure 2: Effect of Solder Voids on Heat flow. Increase in Solder Void area with increasing number of Thermal Cycles [15]

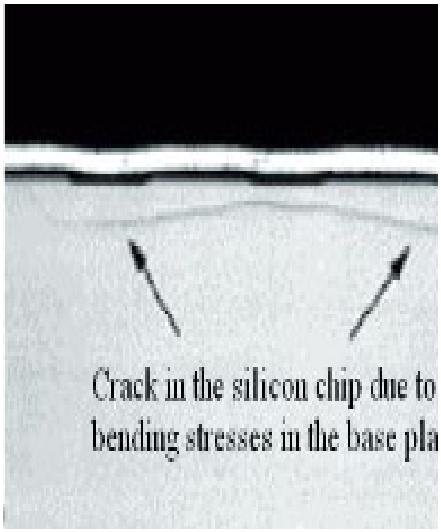

Figure 3: Cracks in Unstressed DBC Substrate [16]

2.4 Reconstruction of the Al Metallization

In order to create a bondable metal layer that can be used to create electrical connections between chips and external connectors or between chips and other chips using bond wires, a thin layer of aluminum with a thickness of 3 to 8 m must be deposited onto a silicon substrate or semiconductor material [17]. Reconstruction is the extrusion of aluminum

grain and the production of hillocks and gaps on thin films, resulting in a rough surface due to the mismatch in CTEs between silicon and aluminum. Figure 5 depicts the reconstruction of the aluminum metallization for an IGBT.

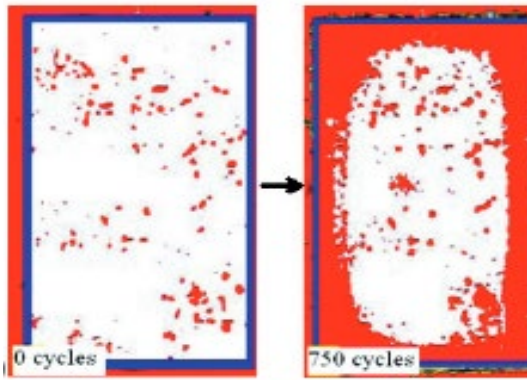

Figure 4: Delamination progression as a result of Temperature Cycling [16]

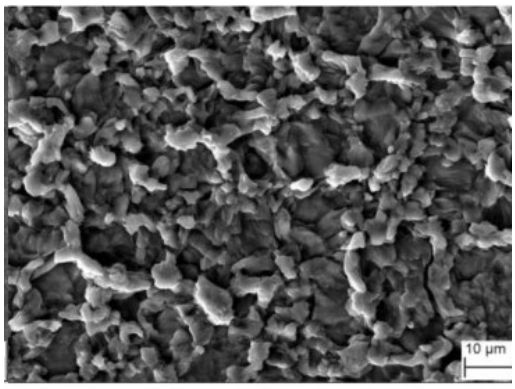

Figure 5: Surface morphology of Al Metallization of IGBT [17]

2.5 Electro-migration

Electro-migration is the movement of atoms based on the flow of electric current through a material. High current densities in the range of 10^6 to 10^7 Acm^{-2} in power devices are always paired with temperature gradients, which significantly enhances electro-migration and shortens the lifetime of power devices [18]. Figure 6 shows the present of hillock and crystalline formation due to electro-migration.

2.6 Die Fracture

Figure 7 shows how tensile loads can cause fractures to occur by stable fatigue propagation to critical sizes large enough to result in brittle failure of the die [19]. This results from the mismatch between the silicon and substrate CTEs, which happens during power and temperature cycling.

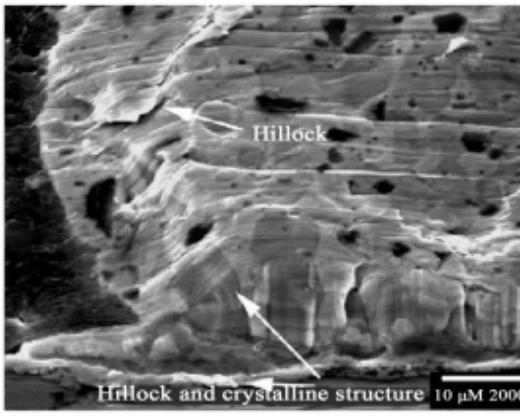

Figure 6: Hillock and crystalline formation due to power cycling [18]

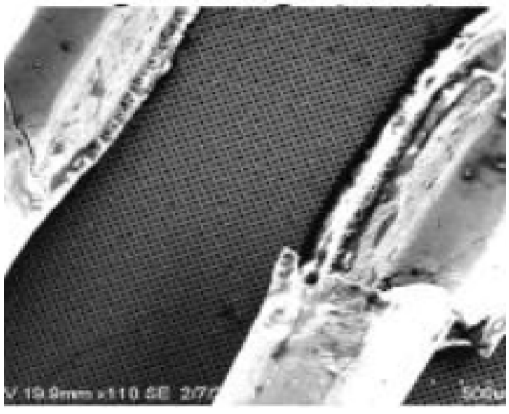

Figure 7: Bond Wire Fracture [19]

3.0 HEAT SINK MODEL

Prior to selecting a heat sink, it is critical to classify the air flow as natural, low flow or high flow forced convection. A heat sink should be created utilizing the natural convection criterion index for the best circumstances and performance [20-21]. The volume of a heat sink is determined using equation (1):

$$V = \frac{P_d \times R_v}{T_j - T_a} \tag{1}$$

Where P_d is the power dissipated, W; R_v is the volumetric thermal resistance, cm^3 °C/W and T_j and T_a are the junction and ambient temperature respectively °C. The power dissipation is a summation of power loss due to conduction and turn and turn of power losses defined as equation (2):

$$P_d = P_{cond} + P_{on} + P_{off} \tag{2}$$

Where

$$P_{cond} = I_D^2 \times R_{DSON} \times D \tag{3}$$

$$P_{on} = E_{on} \times f_{sw} \tag{4}$$

$$E_{on} = \frac{I_D \times V_D \times t_{on}}{2} \tag{5}$$

$$t_{on} = t_{ri} + t_{fu} \tag{6}$$

$$P_{off} = E_{off} \times f_{sw} \tag{7}$$

$$E_{off} = \frac{I_D \times V_D \times t_{off}}{2} \tag{8}$$

$$t_{off} = t_{ri2} + t_{fu2} \tag{9}$$

Range of volumetric thermal resistance is detailed in table 1.

Table 1: Values of Volumetric Thermal Resistance [22]

Flow conditions /m/s	Natural convection	1.0	2.5	5.0
Volumetric resisrance / cm^3 °C/W	500-800	150-250	80-150	50-80

3.1 Entropy Generation

Entropy generation is a notion that is frequently utilized in thermal optimizations because it quantify the irreversibility of a thermal process. The irreversibility can be gauged using a function known as the Lyapovnov function [23]. It is anticipated that as a system performance increases, entropy creation will also decrease because a drop in entropy equals a decrease in irreversibility. Free convection entropy generation for a heat sink is obtain using equation (10) [23]:

$$S_{gen} = \frac{P_d \theta_b}{T_a^2} \tag{10}$$

Where θ_b equal excess temperature of the heat sink base plate °C, expressed using equation (11)

$$\theta_b = P_d \times R_{sink} \tag{11}$$

The overall thermal resistance of the heat sink, R_{sink}, °C/W, is gotten using equation (12):

$$R_{sink} = R_{total} + R_{base} \tag{12}$$

Where R_{total}, the total thermal resistance of fins and exposed base plate, °C/W; R_{base}, the thermal resistance of the heat sink base.

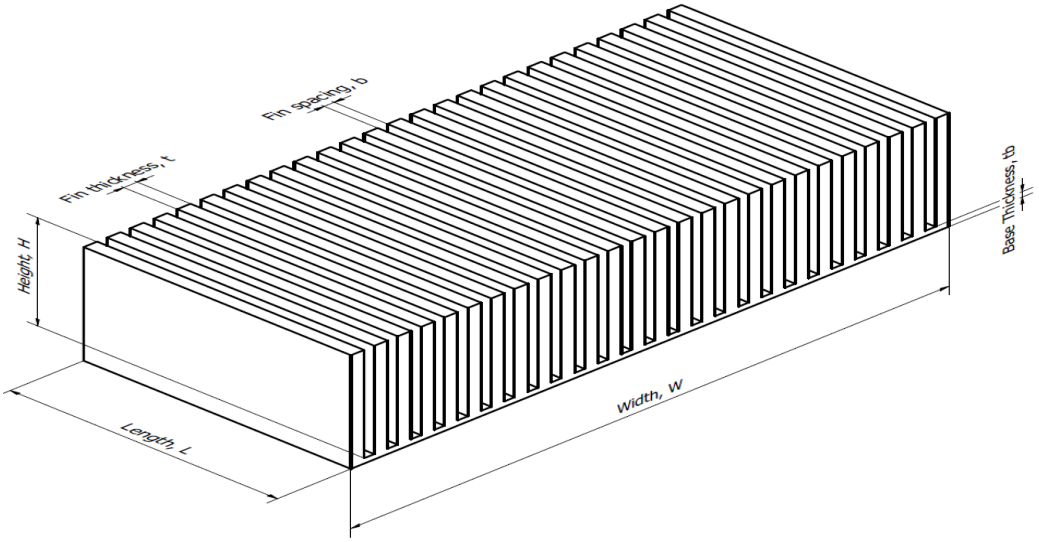

Figure 8: Heat Sink Geometry

Considering the geometry of the heat sink shown in figure 8, R_{total} , which is determined by the total thermal resistance produced by the exposed base plate and fins is define by equation (13) [23]:

$$R_{total} = \frac{1}{\frac{n}{R_{fin}} + hbL(n-1)} \tag{13}$$

Where n equal number of fin, h the heat transfer coefficient, $Wm^{-2}K^{-1}$; b the fin spacing, m; L the length of the heat-sink, m; R_{fin} the thermal resistance of a single fin.

The thermal resistance of a fin is defined by equation (14):

$$R_{fin} = \frac{1}{\sqrt{hPK_aA_c}tanh\,(mH)} \tag{14}$$

Where

$$m = \sqrt{\frac{hP}{K_aA_c}} \tag{15}$$

$$A_c = Lt \tag{16}$$

$$P = 2(L + t) \tag{17}$$

Where t equal fin thickness, m; k_a the thermal conductivity of air, $Wm^{-1}K^{-1}$; m the fin parameter; A_c the cross section area of fin, m^2; P the circumference of fin, m.

The bulk of heat sink material's thermal resistance base R_{base}, is obtain using equation (18):

$$R_{base} = \frac{t_b}{kLW} \tag{18}$$

Where t_b equal base thickness, m; k the thermal conductivity of heat sink material, W/mk; W the heat sink width, m.

In the light of equations (11-18), the entropy generation can be expressed as equation (19):

$$S_{gen} = \frac{P_d\left(P_d \times \left(\left(\frac{1}{\frac{n}{R_{fin}} + hbL(n-1)}\right) + \left(\frac{t_b}{kLW}\right)\right)\right)}{T_b^2} \tag{19}$$

The heat transfer coefficient of the straight fin heat sink under natural convection is obtain using equation (20) [23]:

$$h = \frac{K_a}{b}\left[\frac{576}{EI^2} + \frac{2.873}{EI^{0.5}}\right]^{-0.5} \tag{20}$$

Where EI equal Elenbaas number and can be evaluated using equation (21):

$$EI = \frac{\rho^2 \beta g C_p b^4 \underline{\theta}}{v_f K_a L} \tag{21}$$

Where C_p equal specific heat capacity at constant pressure of air, kJ/kgK; g the gravitational acceleration, m/s^2; ρ the density of air, kg/m^3; v_f the dynamic viscosity of air, m^2/s; β the coefficient of thermal expansion for air, 1/K; $\underline{\theta}$ the average temperature difference across the heat sink.

3.2 Particle Swarm Optimization (PSO)

Population base computing strategy called Particle Swarm Optimization (PSO) was first introduced by Kennedy and Eberhart [24]. The population of solutions, or swarm in this context, is made up of a number of particles. Each particle in the swarm is considered as a point in the dimensional search space, which modifies its position based on its own flight experience and that of the other particles in the swarm. The method determines the particles' next positions in the search space using their current movement, personal experience and collective experience. Additionally, two variables c1 and c2 and two random values created between [0, 1] speed up the experiences, while an inertia factor w fluctuating between $[w_{min}, w_{max}]$ multiplies the current movement, [25]. The objective function for this PSO analysis is defined as the rate of entropy generation, which can be expressed as:

$$S_{gen} = f(n, t, H, b, t_b) \tag{22}$$

The function's goal is to reduce the rate at which entropy is generated. The following are the settings for MATLAB's consideration of linear and nonlinear inequality constraints.

$$g_1: \frac{(L-nt)}{(n-1)} - 0.010 \leq 0 \quad (23)$$

$$g_2: \frac{H(n-1)}{(L-nt)} - 10 \leq 0 \quad (24)$$

$$g_3: \frac{1-H(n-1)}{(L-nt)} \leq 0 \quad (25)$$

$$g_4: \frac{tb(n)}{(L-b)} - 0.8 \leq 0 \quad (26)$$

$$g_5: \frac{1-(tb*n)}{(L-b)} - 0.3 \leq 0 \quad (27)$$

g_1 Indicate that the fin gap should be fewer than 10 mm. Due to the limited installation space, two limitations regarding g_2 and g_3 suggest that the ratio of the fins' height to thickness should fall between 1 and 10. g4 and g5 suggest that the ratio of the base thickness to fin thickness should fall between 0.3 and 0.8. The lower and upper bound of number of fins, fin thickness, fin height and base thickness are respectively defined by equations (28), (29). (30), (31) and equation (32) respectively.

$$g_6: 10 \leq n \leq 30 \quad (28)$$

$$g_7: 0.004 \leq t \leq 0.01 \quad (29)$$

$$g_8: 0.04 \leq H \leq 0.07 \quad (30)$$

$$g_9: 0.002 \leq tb \leq 0.006 \quad (31)$$

$$g_{10}: 0.003 \leq tb \leq 0.01 \quad (32)$$

Implementation of right fitness function is defined using equation (33):

$$fitness = \{S_{gen}\ S_{gen} + C \quad (33)$$

Where the penalty constant, C, has been configured to 1000. When a solution satisfies the constraint of the structural size of the plate-fin heat sink, the rate of entropy creation equates to the fitness function. The value of the fitness function is equivalent to the sum of the entropy generation rate and the penalty constant when a solution does not meet the limitation condition.

The modelled heat sink thermal performance is to be evaluated using Computational Fluid Dynamics (CFD). The equations solved by CFD are the energy continuity equation define by equation (34):

$$\frac{\partial u}{\partial x} + \frac{\partial v}{\partial y} + \frac{\partial w}{\partial z} = 0 \quad (34)$$

The momentum equation define by equation (35):

$$\begin{cases} \rho\left(u\frac{\partial u}{\partial x}+v\frac{\partial u}{\partial y}+w\frac{\partial u}{\partial z}\right)=-\frac{\partial \rho}{\partial x}+\mu\left(\frac{\partial^2 u}{\partial x^2}+\frac{\partial^2 u}{\partial y^2}+\frac{\partial^2 u}{\partial z^2}\right) \\ \rho\left(u\frac{\partial v}{\partial x}+v\frac{\partial v}{\partial y}+w\frac{\partial v}{\partial z}\right)=-\frac{\partial \rho}{\partial x}+\mu\left(\frac{\partial^2 v}{\partial x^2}+\frac{\partial^2 v}{\partial y^2}+\frac{\partial^2 v}{\partial z^2}\right) \\ \rho\left(u\frac{\partial w}{\partial x}+v\frac{\partial w}{\partial y}+w\frac{\partial w}{\partial z}\right)=-\frac{\partial \rho}{\partial x}+\mu\left(\frac{\partial^2 w}{\partial x^2}+\frac{\partial^2 w}{\partial y^2}+\frac{\partial^2 w}{\partial z^2}\right) \end{cases} \quad (35)$$

And the energy equation define by equation (36):

$$u\frac{\partial T}{\partial x}+v\frac{\partial T}{\partial y}+w\frac{\partial T}{\partial z}=\frac{1}{\alpha}\left(\frac{\partial^2 T}{\partial x^2}+\frac{\partial^2 T}{\partial y^2}+\frac{\partial^2 T}{\partial z^2}\right) \quad (36)$$

4.0 RESEARCH METHOD

This study involves modelling, simulation and experimental testing of a heat sink for a power inverter. The heat sink is modelled and solved using the particle swarm optimization technique in MATLAB to obtain the heat sink geometry. Figure 9 depicts the flow diagram of the PSO algorithm. A model of the heat sink geometry is generated using solid works and the created model is solve numerically using ANSYS Fluent to obtain its thermal response. IRF 3205 MOSFETs are attached to the heat sink and thereafter installed on the casing of a 24 V, 3.5 KVA inverter used to power a 1.5 HP air conditioning unit. The schematic diagram of each of the components comprising the setup is as shown in figure 10. The experimental setup is as shown in figure 11. The battery bank is charged with two photovoltaic modules connected in series through a charge controller. In-door and out-doors conditions are monitored with the aid of 8706 digital psychrometer with an accuracy of $\pm 3\%$ for relative humidity and $\pm 0.6°C$ for temperature measurement at 25°C, solar radiation incident on the PV modules was recorded using with a TM-208 Solar power meter with an accuracy of ± 10 Wm^{-2} and cooling fan speed was measured with an GM-8908 anemometer with an accuracy of $\pm 5\%$. All the instruments were calibrated in house before use.

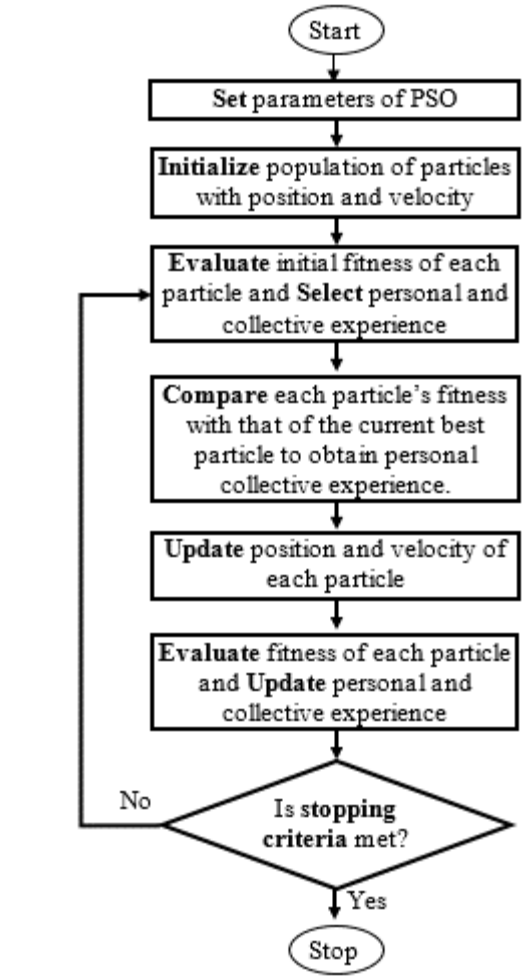

Figure 9: PSO Flow Diagram

Figure 10: Schematic Diagram of Test Rig

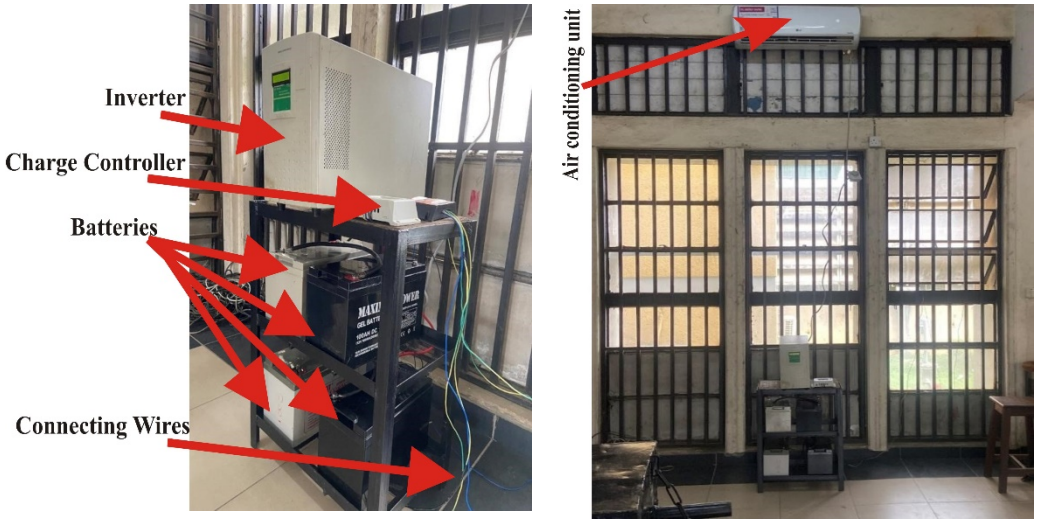

Test Rig

PV Modules

TM-206 Solar Power Meter

8706 Psychrometer

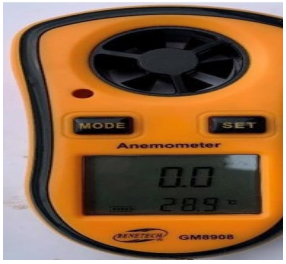

GM-8908Anenometer

Figure 11: Experimental Setup

5.0 RESULTS AND DISCUSSION

5.1 Numerical Simulation

The result of the Particle Swarm Optimization yield the parameters of the heat sink geometry as number of fins 20, fin thickness 4 mm, fin height 40 mm, fin spacing 3 mm and heat sink base thickness 2 mm. A model of the heat sink is created in ANSYS fluent design modeler as shown in figure 12 with a view to determining its thermal response. The input parameters are heat flux from the MOSFETs switches, air velocity, ambient temperature and pressure differential along the heat sink width.

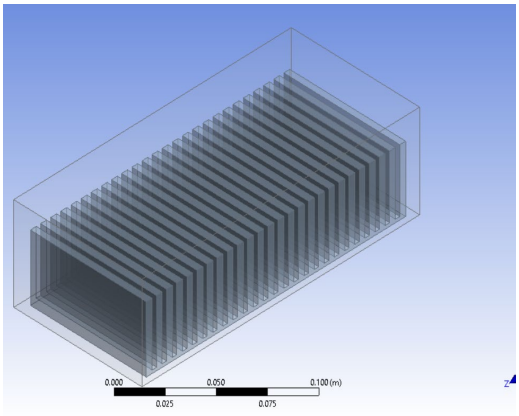

Figure 12: CAD Model in ANSYS Design Modeler

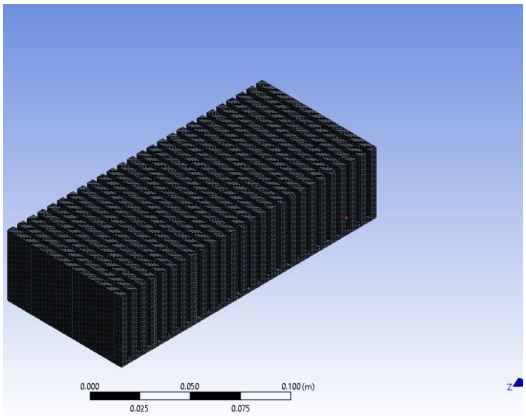

Figure 13: Heat sink mesh

Mesh was generated using hexahedral elements of size 1 mm, linear element order with adaptive sizing settings enabled to dynamically refine the mesh based on geometry for computational efficiency and accuracy. The quality focus of the mesh was orthogonal and skew-ness ratio with an average value 0.8, are considered good and adequate for accurate CFD simulations, with a total of 941899 nodes and 3482703 Elements. Skew-ness ratio ensured well shaped elements while orthogonal quality minimizes distortion, both contributing to the overall reliability of the mesh [26-27]. Figure 11 shows the messed heat sink model. Finally, the solution is initialized using hybrid initialization and solved for 500 iterations. Figure 14 shows the thermograph at a maximum dissipated power of 200 W using IRF 3205 MOSFETs data sheet to estimate the heat flux yielding a base heat sink temperature of 175°C. Figure 15 shows the thermograph obtained using dissipated power of 45 W obtained when the inverter is used to power the 1.5 HP air conditioning unit as recorded by 1602 A LCD after two hours of steady operation, yielding a maximum base heat sink temperature of 69°C.

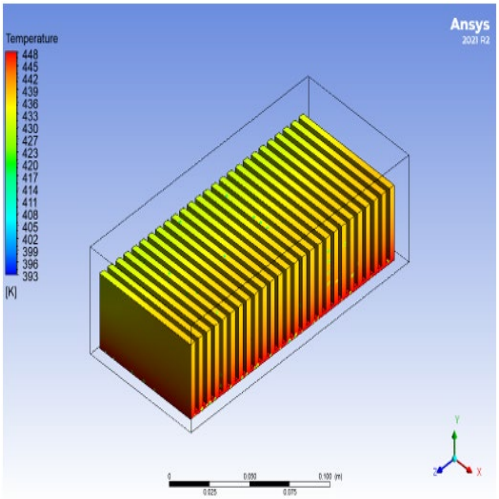

Figure 14: Thermograph 200 W

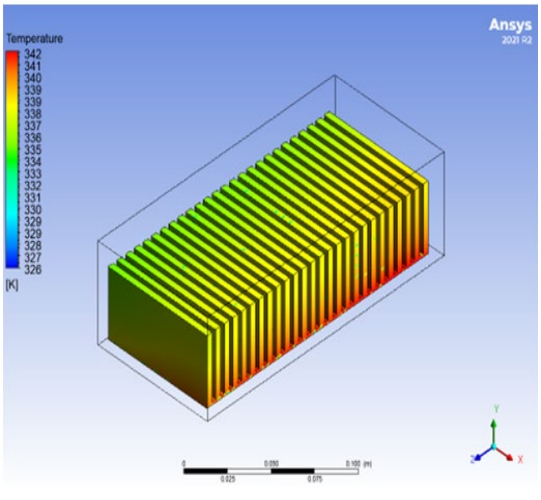

Figure 15: Thermograph 45 W

5.2 Experimental Results

Figure 16 present plots of outdoor and indoor wet and dry bulb temperatures with respective to time. As expected the dry bulb temperatures lead the wet bulb temperatures for the indoor and outdoor air. The indoor dry bulb and wet bulb temperature decreases readily due to the cooling effect of the air-conditioning unit.

Figure 17 shows the plot of the heat sink base temperature and solar radiation with time. Clearly the heat sink base temperature increases steadily with time as expected reaching a maximum of 64°C. The maximum simulated heat sink base temperature was 69°C, yielding a percentage difference of 5%. The prevailing atmospheric condition has a maximum solar radiation of 195 W/m^2 which is significantly low and account for the near convergence of dry bulb and wet bulb temperature of the outdoor air shown in figure 16.

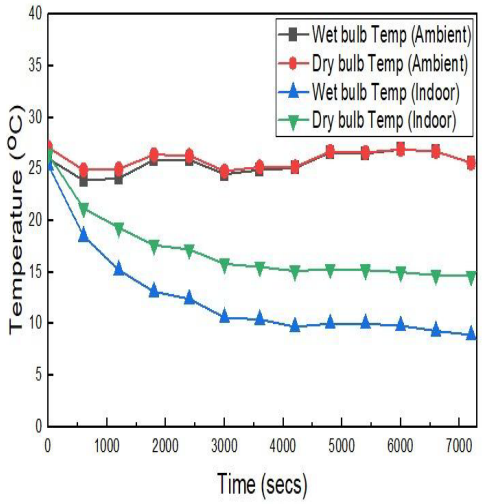

Figure 16: Indoor and Outdoor temperature (wet bulb and dry bulb) vs Time

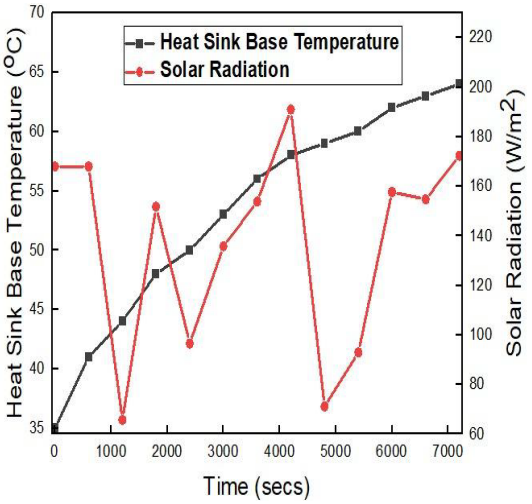

Figure 17: Heat sink base temperature and Solar Radiation vs Time

6.0 CONCLUSION

The primary purpose of power inverters is to provide energy for modern civilization in a more effective, sustainable, and manageable way. Issues with power inverter reliability are mostly caused by thermally induced failure caused majorly by differences in coefficient of thermal expansion of the materials used in making the AC to DC power modules thus necessitating the need for a heat sink. A heat sink was subsequently created and optimized using MATLAB's particle swarm optimization (PSO) technique with the goal of effectively dispersing the heat produced by the power inverter to ensure safe operation and to prolong the life of the inverter. The modelled heat sink has; number of fins, fin thickness, fin height, fin spacing, and fin base thickness of 26, 4mm, 40mm, 3mm and 2 mm. The thermal performance of the optimized heat sink was simulated using CFD and then experimented with a 24 V 3.5 KVA power inverter operating a 1.5 HP air-conditioning unit. Results show a maximum simulated and experimental heat base temperature of 67.85°C and 64°C with a dissipated power of 45 W, with a 6.02% deviation.

References

[1] Li J., Yang L. (2023). Recent Development of Heat Sink and Related Development of Heat Sink and Related Design Methods. *Energies*, 16, 7133: 1-23.

[2] Wong M., Owen I., Sutcliffe C. J., Puri A. (2009). Convective Heat Transfer and Pressure Losses across Novel Heat Sinks Fabricated by Selective Laser Melting. *International Journal of Heat Mass Transfer*, 52: 281–288.

[3] Prabhakar P. S., Ghuge N. C. (2015). Thermal Design and Analysis of Heat Sink Optimization and its Comparison with Commercially Available Heat Sink. *International Journal of Engineering Research and Technology*, 4(12): 210 - 216.

[4] Ekpu M., Bhatti R., Ekere N., Mallik S., Amalu E,. Otiaba K. (2011). Investigation of Effects of Heat Sinks on Thermal Performance of Microelectronic Package, *3rd IEEE International Conference on Adaptive Science and Technology (ICAST)*, Chatham,Kent,United Kingdom: 127-132.
[5] Onoroh F., Adewumi O. O., Ogbonnaya M. (2019). Characterization of a Finned Heat Sink for a Power Inverter. *Journal of Physics: Conf. Series*: 1-15.
[6] Chinthavali M. S., Wang Z. J. (2018). 30-kW All-SiC Inverter with 3D-Printed Air-Cooled Heatsinks for Plug-in and Full Electric Vehicle Applications. *Oak Ridge National Laboratory*, US Department of Energy.
[7] Jonsson H., Moshfegh B. (2001). Modeling of the Thermal and Hydraulic Performance of Plate Fin, Strip Fin, and Pin Fin Heat Sinks-Influence of Flow Bypass. Components and Packaging Technologies. *IEEE Transactions*, 24(2): 142-149.
[8] Arularasan R., Velraj, R. (2008). CFD Analysis in a Heat Sink for Cooling of Electronic Devices. *International Journal of the Computer, the Internet and Management*, 16(3): 1-11.
[9] Shadlaghani A., Tavakoli, M. R., Farzaneh M. Salimpour M. R. (2016). Optimization of Triangular Fins with and without Longitudinal Perforate for Thermal Performance Enhancement. *Journal of Mechanical Science and Technology*, 30(4): 1903-1910.
[10] Jaffal H. M. (2017). The Effect of Fin Design on Thermal Performance of Heat Sink. *Journal of Engineering*, 5(23): 123–146.
[11] Ibrahim T. K., Mohammed M. N., Mohammed M. K., Najafi, G., Sidik N. A. C., Basrawi F., Abdalla A. N., Hoseini S. S. (2018). Experimental Study on the Effect of Perforations Shapes on Vertical Heated Fins Performance under Forced Convection Heat Transfer. *International Journal of Heat Mass Transfer*, 118: 832–846.
[12] Kulkarni V. M., Dotihal B. (2015). CFD and Conjugate Heat Transfer Analysis of Heat Sinks with Different Fin Geometries Subjected to Forced Convection used in Electronics Cooling. *International Journal of Research in Engineering and Technology*, 4(6): 158-163.
[13] Mjallal I., Farhat H., Hammoud M., Ali S., Shaer A.A., Assi A. (2018). Cooling Performance of Heat Sinks used in Electronic Devices. MATEC Web of Conference, 171: 1-4.
[14] Luo J., Guan S., Wan B., Jiang M., Fu G. (2021). Research on IGBT Bonding Wires Crack Propagation at Macro and Micro Scales. *IEEE Access*, 9: 106270-106282.
[15] Shammas N. Y. A. (2003). Present problems of Power Module packaging technology. *Microelectronics reliability*, 43(4): 519-527.
[16] Zeanh A., Dalverny O., Karama M., Woirgard E., Azzopardi S., Bouzourene A., Casutt J., Mermet-Guyennet. (2008). Reliability of the connections used in IGBT modules in aeronautical environment. *International Journal for Simulation and Multidisciplinary Design optimization*, 2: 123-133.
[17] An T., Zheng X., Qin F., Dai Y., Gong Y., Chen P. (2023). Macro-Mesoscale Modeling of the Evolution of the Surface Roughness of the Al Metallization Layer of an IGBT Module during Power Cycling. *Materials*, 16(5): 1936.
[18] Rahman M. K., Musa A. M. M., Neher B., Patwary K. A., Rahman M. A., Islam M. S. (2016). A Review of the Study on the Electro-migration and Power Electronics. *Journal of Electronics Cooling and Thermal Control*, 6: 19-31.
[19] Lall P., Pecht M.G., Hakim E.B. (2020). *Influence of Temperature on Microelectronics and System Reliability: A Physics of Failure*. CRC Press London.
[20] Jasim H. H. (2020). Development of Natural Convection Heat Transfer in Heat Transfer using a New Fin Design. *Journal of Mechanical Engineering Research and Development*, 43(3).
[21] Habib N., Siddiqi M. U. R., Tahir M. (2020). Thermal Analysis of Proposed Heat Sink Design under Natural Convection for the Thermal Management of Electronics. *Thermal Science*, 26(2B): 1487-1501.
[22] Lee S. (1995). Optimum Design and Selection of Heat Sinks. *IEEE Transactions on Components, Packaging, and Manufacturing Technology: Part A*, 18(4): 812-817.
[23] Bhandari, V. S.,Kulkarni, S. H. (2019). Optimization of Heat Sink for Thyristor Using Particle Swarm Optimization. *Results in Engineering*, 4: 1-4.
[24] Kennedy, J., Eberhart, R., (1995). Particle Swarm Optimization. *Proceedings IEEE International Conference Neural Network*: 1942-1948.
[25] Pratihar D. K. (2015). *Soft Computing Fundamentals and Applications*. Revised edition, Alpha Science International Limited, Oxford: 87-88.
[26] Versteeg H. K., Malalasekera W. (2007). *An Introduction to Computational Fluid Dynamics:Finite Volume Method*. 2nd Edition, Pearson Education Limited, England: 1-7.
[27] ANSYS FLUENT 12.0 User's Guide (enea.it). [Accessed: 10th November, 2023].